Electrocatalysis at Single Nanoparticles

Kleijn, S.E.F.

5

Landing and Catalytic Characterization of Individual Nanoparticles on Electrode Surfaces

Abstract

We demonstrate a novel and versatile pipet-based approach to study the landing of individual nanoparticles (NPs) on various electrode materials, without any need for encapsulation or fabrication of complex substrate electrode structures, providing great flexibility with respect to electrode materials. Due to the small electrode areas defined by the pipet dimensions, the background current is low, allowing for the detection of minute current signals with good time resolution. This approach was used to characterize the potential-dependent activity of Au NPs and to measure the catalytic activity of a single NP on a TEM grid, combining electrochemical and physical characterization at the single NP level for the first time. Such measurements open up the possibility of studying the relation between size and activity of catalyst particles unambiguously.

5.1 Introduction

Metal nanoparticles (NPs) have been extensively studied as electrocatalysts in numerous fields and applications.[1–3] A key aspect of NPs is their size- and structure-dependent reactivity,[2] which is often inferred from 'top-down' studies of ensembles of catalytic NPs. However, due to the inherent variance in NP size and shape, only average reactivity trends may be obtained in this way. Even when one can work with a narrow size distribution, subtle effects may substantially alter reactivity. Indeed, we have shown in a previous study that ostensibly similar NPs can have very different reactivity due to subtle variations in morphology.[4] Therefore, to truly understand NP reactivity on a fundamental level, it is imperative to study single NPs. While such an investigation is demanding, as it requires placing, locating and characterizing a single NP, a few experimental studies have been reported.[4–13] Single NP studies are further challenging due to the need for high accuracy measurement of the small (current) signals with reasonable bandwidth.[13–15]

A recent innovative method to electrochemically detect individual NPs[7–12] focuses on NPs that are dispersed in an electrolyte solution, that can diffuse to, and land on, an electrode surface held at a potential where a reaction occurs on the catalytic NP but not on the inert collector electrode. Consequently, arrival of a NP at the electrode surface results in an increase in current due to the NP reaction, which can be a reaction of a species in solution[7] or the oxidation of the NP itself.[10] In order to limit the number of NPs landing and minimize the background current, a collector electrode of small area is needed. The preparation of such ultra-microelectrodes (UMEs) greatly limits the choices of substrate material, since not every material (particularly material of practical importance) can be shaped to micro- or nanoscale dimension, and even when the material can be encapsulated, electrode preparation requires considerable time and effort.[16–18] A typical UME (~5 µm diameter) often still shows a considerable background signal compared to the electrochemical signal from the NP reaction.[7–12] Consequently, only large current signals (often resulting from mass transport limited reactions)[7, 9]can be detected, and obtaining an entire current-voltage response at an individual NP has so far proved impossible. Furthermore, subsequent characterization of immobilized NPs has proven very challenging.[17]

In this chapter, we demonstrate the study of single NP reactivity by employing scanning electrochemical cell microscopy (SECCM) to select and isolate a small area on a collector eletrode, of any kind of material, and to land, detect and characterize individual NPs. The experimental set-up is schematically depicted in Figure 5.1a and

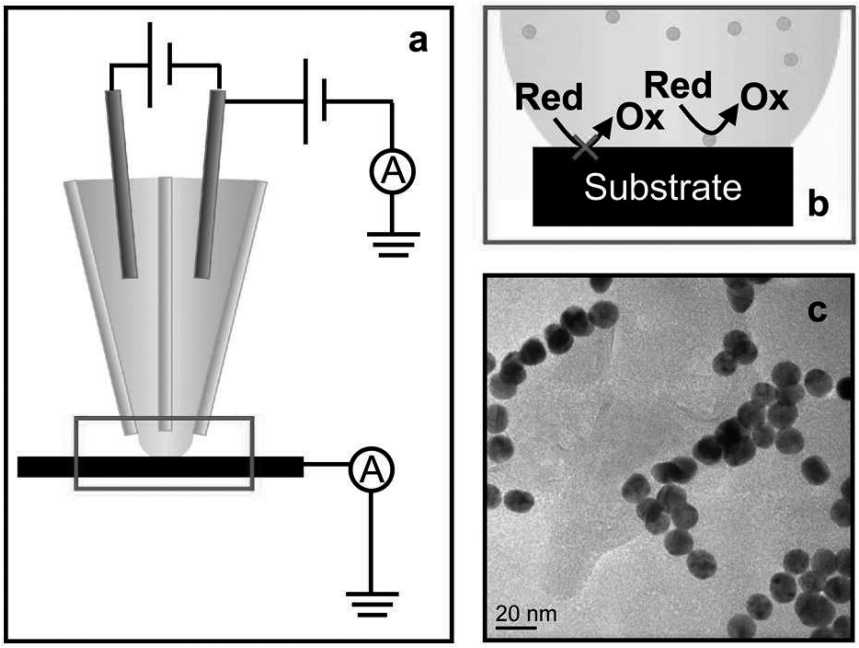

Figure 5.1: (a) Schematic of the experimental setup. (b) Schematic of the liquid meniscus constituting the electrochemical cell. The substrate is held at a potential where a reaction occurs on the catalytic AuNP, but not on the collector electrode. (c) TEM image of the AuNPs used in this study.

b and described in full in the Experimental section. In short, a dual-channel (theta) pipet with a sharp point of approximately 1.5 µm diameter was filled with an electrolyte solution of interest (containing ~70 pM citrate-capped gold NPs (AuNPs), 10-20 nm diameter,[19, 20] Figure 5.1c) and two palladium-hydrogen (Pd-H_2; E^0 = 50 mV vs. reversible hydrogen electrode, RHE)[4] quasi-reference counter electrodes (QRCEs), both held at the same potential. All potentials throughout this study are reported relative to the RHE. The use of a theta pipet allowed us to monitor the size of the liquid meniscus formed at the end of the pipet by measuring the ionic current between the two QRCEs across the meniscus when a small potential bias was applied between them. Furthermore, the migration rate of charged species can be controlled by the bias potential applied between the QRCEs,[21] but this option was not employed in this work. The pipet was mounted on a piezoelectric positioning system and slowly lowered towards the substrate, which was held at ground, while the current flowing through the substrate was monitored continuously. Upon contact of the liquid meniscus at the end

of the pipet with the substrate, a current spike was observed at the substrate due to the formation of the electrical double layer. This was used to automatically halt the approach so that the pipet was held in place for the duration of the experiment. The resulting meniscus between the pipet and substrate constitutes a micro- or nanoscopic electrochemical cell with the wetted area of the substrate as working electrode, which experiences a potential of the same magnitude but opposite sign as the potential applied to the QRCEs. In this approach, we isolate an area on the working electrode by limiting the electrolyte contact (rather than by decreasing the size of the working electrode, as in previous studies[7–12]), which results in at least three main advantages. First, this allows the use of a wide range of electrode materials, size and morphologies, as no traditional UME manufacture is required, instead relying on facile micro- or nanopipet preparation. Second, we can make and break the cell at will on a specific site on the electrode surface (on a millisecond timescale if needed), by simply moving the pipet away from or towards the substrate. This is particularly beneficial if one wishes to land single NPs in a predetermined pattern. Finally, the working electrode area in this pipet-based approach is determined by the size of the pipet,[21, 22] which can be routinely prepared to be smaller than a typical UME (of several micrometers in diameter), down to <200 nm.[23] Such ultra-small surface areas result in a significant decrease in background current (by two orders of magnitude) compared to the UMEs presently used, allowing detection of much smaller currents from the NP reaction itself.

5.2 Experimental

5.2.1 Setup

The experiments were conducted on a scanning electrochemical cell microscopy (SECCM) [24] set-up.[22] The pipet was a dual channel probe pulled from a borosilicate theta glass capillary (TGC150-10, Harvard Apparatus) using a CO_2-laser puller (P-2000, Sutter Instruments) to a sharp taper of approximately 1.5 µm total diameter (ca. 700 nm per channel) at the end. The resulting pipet tip was silanized with dichlorodimethylsilane ($Si(CH_3)_2Cl_2$, Acros Organics, 99+%) to render the outer wall hydrophobic. Each channel was filled with the electrolyte solution of interest. A palladium-hydrogen ($Pd-H_2$) quasi-reference counter electrode (QRCE), prepared by evolving hydrogen on a palladium wire (Mateck, 99.9%) in 0.1 M H_2SO_4 (Aldrich, 99.999%) until saturated, was inserted into each channel, and both $Pd-H_2$ QRCEs were held at the same potential. The pipet was mounted on a high-dynamic z-piezoelectric positioner

(P-753.3CD LISA, PhysikInstrumente), while the sample was mounted on a high-precision xy-piezoelectric stage (P-622.1CL PIHera, PhysikInstrumente or P-622.2CL PIHera, PhysikInstrumente). Rough positioning of the pipet and of the sample was aided by two digital CMOS cameras (PL-B776U and PL-B782U, PixeLINK) and a 3-axis micropositioner (Newport), allowing lateral pipet positioning within ca. 10 µm of the point of interest.[4] The entire assembly was installed in a Faraday cage. The pipet was slowly moved to the substrate surface, and the motion was halted when meniscus contact was established, typically evident from a current spike flowing through the substrate due to double layer charging. Current measurements were performed using high sensitivity home-built current to voltage converters. Tip and sample positioning and data acquisition were performed using a FPGA card (PCI-7830R, National Instruments) with a LabVIEW 9.0 interface. Two electrolyte solutions were employed in this study. For the studies on HOPG (ZYA-grade, NT-MDT), a 10 mM phosphate buffer solution (pH 7.2) was prepared by diluting stock phosphate buffer solution (Aldrich) with ultra-pure water (Purite Select system, resistivity 18.2 MΩ cm at 25 °C), to which ~70 pM AuNPs was added. For the studies on the carbon coated Cu TEM grid (carbon film on 400 copper mesh), a 50 mM citrate buffer solution (pH ~4.5) was prepared from 25 mM citric acid (Aldrich, $>$99.5%) and 25 mM trisodium citrate (Aldrich, USP testing standard) and ultra-pure water, to which 2 mM hydrazine sulfate (Sigma Aldrich, ACS reagent, > 99.0%) and ~70 pM AuNPs was added. The TEM grids were treated in an oxygen plasma (Emiteck K1050X Plasma Etcher/Asher/Cleaner) at 100 W for 15 seconds before use to increase the hydrophilicity of the carbon film.

For the landing experiments on the carbon coated Cu TEM grid, the pipet was located on a specific section (square region between the mesh) of the grid using the camera positioning system. To aid locating the particle, only one single NP was deposited per section.

TEM images were recorded on Jeol 2000FX Transmission Electron Microscope at 200 keV accelerating voltage.

5.2.2 Gold nanoparticle synthesis

Gold nanoparticles were prepared following a modified method originally introduced by Turkevich.[19, 20] All glassware used in this procedure was cleaned with fresh aqua regia solution (3:1 concentrated hydrochloric acid (Fischer, lab reagent grade)/ concentrated nitric acid (Aldrich, Volumetric standard)) and thoroughly rinsed with ultra-pure water. In a typical synthesis, 8 ml of 1 mM $HAuCl_4$ (Aldrich, 99.999%) solution was brought to 85 °C and stirred vigorously. 0.8 ml of 38.8 mM trisodium citrate (Aldrich,

USP testing standard) was rapidly added to the vortex of this solution. The solution was held at 85 °C for 10 minutes, then allowed to cool to room temperature with continuous stirring for ~20 minutes. The solution was stored at 4 °C until use. Before use, the nanoparticle solution was stirred in an ultra-sonic bath for at least 30 minutes to obtain a well-dispersed, homogenous solution. TEM measurements show that this results in particles of 10-20 diameter, in agreement with literature values.3

The NP concentration can be estimated as follows: Based on spherical NPs with an average diameter of 16 nm, the mass can be calculated to be 4.14×10^{-17} g/NP, based on a volume of 2.14×10^{-18} cm^3/NP and the bulk density of gold (19.3 g cm^{-3}). Comparing the average mass of one AuNP with the total mass of Au^{3+} precursor (1.58×10^{-3} g Au^{3+}), and assuming full reduction of Au^{3+} to AuNPs, this yields a stock solution 3.81×10^{13} AuNPs in 8.8 ml, or, equivalently, 7.21 nM AuNPs.

5.3 Results

To demonstrate the flexibility of the pipet-based approach, we have landed AuNPs from an aerated 5 mM phosphate buffer solution (pH 7.2) on highly oriented pyrolytic graphite (HOPG) at various potentials. HOPG is an interesting substrate as it serves as a model for novel sp^2 carbon materials and there has been recent debate on the active sites for electron transfer.[22] Furthermore, the surface of HOPG is easily refreshed (through cleaving with adhesive tape) and has low background currents, making it an attractive collector electrode for NP landing experiments.

Typical current-time plots obtained for the landing of AuNPs on HOPG at various potentials (Figure 5.2a-d) show a few general trends. Initially, as the pipet is suspended in air, the recorded substrate current is zero. Once the liquid meniscus is brought into contact with the substrate, the electronic circuit is closed, leading to an initial current spike at all potentials (e.g. at ~90 s. in Figure 5.2a). This current spike can be attributed to the formation of the electric double layer on the HOPG substrate, and its direction is indicative of the potential applied to the substrate relative to its potential of zero total charge (pztc). Given the flexibility of this technique, this finding also opens up possibilities to quickly probe the pztc of a material at the nanoscale under various experimental conditions. Once the meniscus is in contact with the substrate, discrete current steps were observed at potentials at which electrochemical reactions occur on Au but not on HOPG, indicating the arrival of distinct AuNPs. Three potential regimes can be distinguished: at potentials above 1 V (such as at 1.2 V, Figure 5.2a), the current steps are positive. At potentials below 0.15 V (Figure 5.2c and d), the current

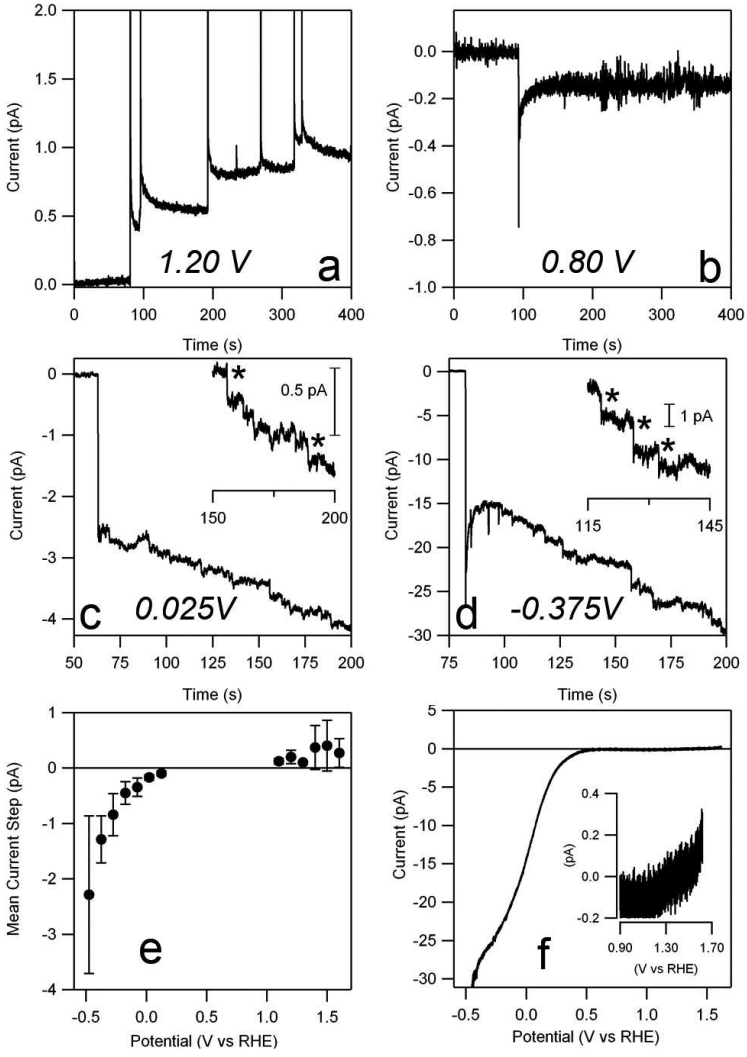

Figure 5.2: (a-d) Current-time plots showing the landing of the pipet meniscus (initial spike) and AuNPs (subsequent steps) at selected potentials. (e) Mean current step height determined as a function of substrate potential. Error bars denote 2σ. (f)Linear sweep voltammogram (50 mV s^{-1}) of Au in 5 mM phosphate buffer, measured using a pipet of 1.5 µm diameter.

steps are negative, and the magnitude increases with more cathodic potential. Finally, at intermediate potentials (Figure 5.2b), no current steps are observed; instead the current-time profile shows a constant background. To understand this current-potential behavior in more detail, Figure 5.2e shows the mean values of the current steps as a function of substrate potential. There is a clear and strong potential dependence, similar to that of a bulk polycrystalline Au electrode measured using the same pipet setup (Figure 5.2f), although the current densities on the AuNPs are higher due to the much increased mass transport rate at nanostructures in the SECCM set-up.[23] At low potentials (< 0.15 V), the observed current steps can be ascribed to the oxygen reduction reaction (ORR). The onset potential appears to be at a higher overpotential than on bulk Au (~0.4 V), but the apparent difference is likely due to the fact that the current steps at lower overpotential are not sufficiently large to be detected, although we also cannot rule out some kinetic effects at the smaller particle due to the greatly enhanced mass transport rate. At intermediate potentials, in the double layer region of Au, no current steps are observed, as no reaction takes place on the AuNP upon landing. This also indicates that the landing of NPs does not disturb the HOPG double layer significantly, while the charging of the particles themselves was not detected. Finally, at potentials positive of 1.10 V, oxidative current steps are observed. Typically, surface oxide formation takes place in this potential range. However, as this process is limited by the Au surface area, it would lead to current spikes with a finite charge (~5 fC for a 20 nm diameter AuNP),[25] rather than current steps. As the oxidation of carbonaceous species is often found to take place in the Au surface oxidation region,[26] we tentatively attribute the oxidative current steps to the oxidation of residual carbonaceous species in solution, as no special effort was taken to purify the solution and reagents.

The excellent signal to noise ratio in these experiments allowed ready analysis of the frequency at which AuNPs land on the HOPG substrate, as a function of the substrate potential (Figure 5.3). These frequency values were obtained by dividing the counted current steps (marked with an asterisk in insets of Figure 5.2c and 5.2d) by the total runtime of the experiment. At the extreme potentials, the experimentally observed frequency is ~0.05 s^{-1}, lower than the theoretical value of 0.4 s^{-1} predicted by diffusion laws: The theoretical landing frequency of AuNPs at the electrode can be estimated based on equations for a purely diffusive NP flux, based on Fick's diffusion laws.[27] The flux of NPs (j_{NP}, expressed in NP s^{-1}) down the pipet to the substrate electrode is ca. 10% of the flux from an infinite solution towards a disc electrode of the same diameter.[21] The diffusive flux to a disc electrode is given by equation 5.1:

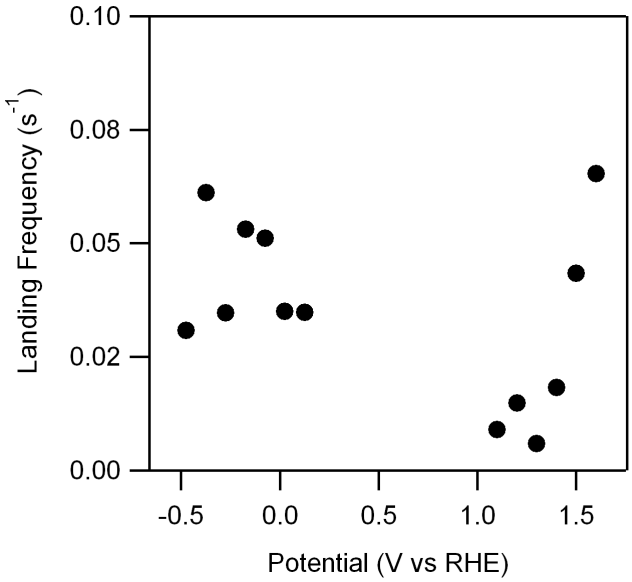

Figure 5.3: Frequency of current steps for landed NPs measured at different potentials.

$$j_{NP} = 4 D_{NP} C_{NP} N_A r_{disc} \tag{5.1}$$

In this equation N_A is Avogadro's constant (N_A = 6.02$\times$ 10^{23} mol^{-1}), r_{disc} is the radius of the disc, and D_{NP} and C_{NP} are the diffusion coefficient of AuNPs and its concentration in solution, respectively. The diffusion coefficient of NPs with radius rNP can be determined from the Stokes-Einstein relation (equation 5.2):

$$D_{NP} = \frac{k_B T}{6\pi\eta r_{NP}} \tag{5.2}$$

in which k_B is the Boltzmann constant (k_B = 1.381 $\times$ 10^{-23} J K^{-1}) and η is the dynamic viscosity of water (η = 8.90 $\times$ 10^{-4} Pa s at 25 ℃). For a 16 nm NP, equation 2 yields a diffusion coefficient of D_{NP} = 3.1 $\times$ 10^{-7} cm^2 s^{-1}. Using this value, we obtain a diffusive flux to a disc with a radius of 750 nm (corresponding to the radius of the pipets employed) of j_{NP} = 3.8 NP s^{-1}, from which we can estimate the theoretical diffusive flux in pipet-based set-up in this study to be $j_{NP} \approx$ 0.4 NP s^{-1}. Experimental landing frequencies have been consistently reported to be lower than predicted from theoretical considerations.[8, 10, 28] Although various explanations have been forwarded to account for this discrepancy, the issue is not yet well understood. Finally, it

should be noted that at moderately high potentials (between 1.0 and 1.5 V), the landing frequency lies below the average. As the magnitude of the current steps is very small in this potential region, we ascribe the diminished observed frequency to the fact that only particularly large or active particles show a catalytic response large enough to be detected, and thus the observed landing frequency may not represent the 'true' landing frequency.

A particularly exciting substrate on which to perform NP landing experiments is a transmission electron microscope (TEM) grid, as this allows characterization of the deposited NPs to fully resolve structure-activity relationships at the level of a single NP. To demonstrate this capability, we have landed AuNPs on a carbon coated TEM grid by measuring the oxidation of 2 mM hydrazine in a 50 mM citrate buffer. Although employing hydrazine with citrate-capped NPs gave rise to some complications (vide infra), it is a good model system for an electrocatalytic reaction, as it is sufficiently facile to reach mass transport limited conditions. Typical landing events, in which the TEM grid was held at 1.25 V (potential close to the mass transport limited regime), are shown in Figure 5.4a. As can be seen, in these experiments, establishing the contact of the meniscus with the carbon film on the TEM grid typically coincides with the landing of the first AuNP, giving rise to current steps of ~40 – 80 pA. The magnitudes of these steps are in good agreement with the current predicted for the diffusion-limited current based on radial diffusion to a sphere with radius r on a plane, as given by equation 5.3.[7]

$$i_{lim} = 4\pi(ln2)nFDCr \tag{5.3}$$

Here n is the number of electrons transferred per hydrazine molecule (4), F is the Faraday constant (9.649×10^4 C mol^{-1}), C is the hydrazine concentration (2 µmol cm^{-3}), and D is the diffusion coefficient of hydrazine. A wide range of diffusion coefficients for hydrazine have been reported, typically $0.5\text{-}1.5 \times 10^{-5}$ cm^2 s^{-1}.[29–31] In this case, we find the best correspondence between the spread in current step magnitudes and AuNP size distribution for $D \approx 1.2 \times 10^{-5}$ cm^2 s^{-1}, a value well within the reported range and typical for small molecules.

The landing frequency was low, with up to tens of seconds between successive landing events, attributable to a much lowered concentration of free AuNPs in solution due to extensive aggregation.[28] This aggregation was observed qualitatively by the color change of a fairly concentrated AuNP solution upon addition of small amounts of hydrazine from pink to gray, followed by AuNP precipitation. Nonetheless, as Figure 5.4 shows, it is still possible to land single AuNPs without interference of aggregates

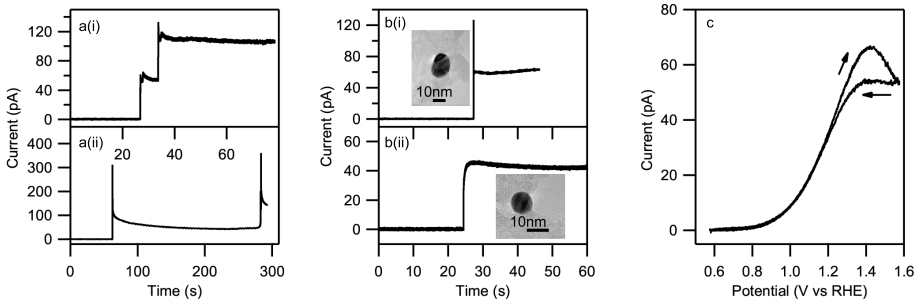

Figure 5.4: (a) AuNPs landing on a carbon coated Cu TEM grid (at 1.25 V) in presence of N_2H_4. (b) Landing events of individual AuNPs, with the same AuNP imaged by TEM afterwards. (c) CV (200 mV s^{-1}) measured at the individual AuNP shown in (b(i)).

landing. This may be due to the fact that the opening at the end of each barrel of the pipet (~700 nm) may be too small for aggregates to pass, thus acting as a particle size filter. The long period between events allowed electrochemical characterization of the AuNP and then retraction of the pipet, leaving the initial AuNP on the TEM grid for subsequent visualization without further AuNPs landing. This made it possible to correlate the electrochemical (current) with the physical properties of the AuNP. Examples are shown in Figure 5.4b: two separate landing experiments were performed with current steps of 40 and 60 pA. Visualizing these same particles with TEM, it can be seen that this difference is directly related to the size difference between the two AuNPs: the current step of 40 pA originating from a ~10 nm NP, while the current of 60 pA originates from a ~15 nm NP, in good agreement with equation (1). This agreement indicates directly that mass transport controls the reactivity of single AuNPs at this potential, and, moreover, the scaling of the current with particle radius confirms that mass transport to a single particle is predominantly radial in nature.

Finally, we were able to sweep the substrate potential after the initial landing event to record a full CV of a single AuNP before retracting the pipet. A CV of the AuNP in Figure 5.4b(ii) is shown in Figure 5.4c. The recorded CV shows an onset potential of ~0.8 V, in good agreement with those reported for hydrazine oxidation on gold electrodes.[32] The oxidation wave is somewhat drawn out compared to CVs recorded on macroscopic Au electrodes,[32] which can be fully ascribed to the increased mass transport coefficient (~6 cm s^{-1}, c.f. ~10^{-3} cm s^{-1} for macroscopic systems) in this configuration.[22]

5.4 Conclusion

In conclusion, we have demonstrated a SECCM-based approach to land and characterize single NPs on electrodes with minimal electrode preparation and the abilooity to select the measurement location. The results obtained with this approach are consistent with previous NP landing studies on UMEs[7–12] but with enhanced sensitivity due to the lower background signals owing to a smaller contact area. As highlighted herein, this pipet-based approach eliminates the need for UME fabrication, and a wide variety of substrates can be investigated. A particularly exciting application has been to use this pipet-based approach to study NP reactivity on a TEM grid, allowing the complete unambiguous correlation of physical and electrochemical properties at a single NP level for the first time. Apart from studying particle size and shape effects, the wide range of substrates that can be studied also opens up the possibility to study substrate effects on electrocatalytic reactions, an aspect which is not yet well-understood. We believe that these prospects make this pipet-based approach particularly powerful for further understanding and resolving nanoparticle reactivity.

Bibliography

[1] Somorjai, G. A. *Science* 1985, *227*(4689), 902–908.

[2] Chen, A.; Holt-Hindle, P. *Chem. Rev.* 2010, *110*(6), 3767–3804.

[3] Koper, M. T. M. *Nanoscale* 2011, *3*, 2054–2073.

[4] Lai, S. C.; Dudin, P. V.; Macpherson, J. V.; Unwin, P. R. *J. Am. Chem. Soc.* 2011, *133*(28), 10744–10747.

[5] Meier, J.; Friedrich, K. A.; Stimming, U. *Faraday Discuss.* 2002, *121*, 365–372.

[6] Krapf, D.; Wu, M.-Y.; Smeets, R. M. M.; Zandbergen, H. W.; Dekker, C.; Lemay, S. G. *Nano Lett.* 2006, *6*(1), 105–109.

[7] Xiao, X.; Bard, A. J. *J. Am. Chem. Soc.* 2007, *129*(31), 9610–9612.

[8] Xiao, X.; Fan, F.-R. F.; Zhou, J.; Bard, A. J. *J. Am. Chem. Soc.* 2008, *130*(49), 16669–16677.

[9] Bard, A. J.; Zhou, H.; Kwon, S. J. *Isr. J. Chem.* 2010, *50*(3), 267–276.

[10] Zhou, Y.-G.; Rees, N. V.; Compton, R. G. *Angew. Chem., Int. Ed.* 2011, *50*(18), 4219–4221.

[11] Kwon, S. J.; Bard, A. J. *J. Am. Chem. Soc.* 2012, *134*(16), 7102–7108.

[12] Rees, N. V.; Zhou, Y.-G.; Compton, R. G. *RSC Adv.* 2012, *2*, 379–384.

[13] Chen, S.; Kucernak, A. *J. Phys. Chem. B* 2003, *107*(33), 8392–8402.

[14] Eikerling, M.; Meier, J.; Stimming, U. *Zeitschrift für Physikalische Chemie* 2003, *217*(4-2003), 395–414.

[15] Hoeben, F. J. M.; Meijer, F. S.; Dekker, C.; Albracht, S. P. J.; Heering, H. A.; Lemay, S. G. *ACS Nano* 2008, *2*(12), 2497–2504.

[16] Cox, J. T.; Zhang, B. *Annu. Rev. Anal. Chem.* 2012, *5*(1), 253–272.

[17] Li, Y.; Cox, J. T.; Zhang, B. *J. Am. Chem. Soc.* 2010, *132*(9), 3047–3054.

[18] Kleijn, S. E.; Yanson, A. I.; Koper, M. T. *J. Electroanal. Chem.* 2012, *666*(0), 19 – 24.

[19] Turkevich, J.; Stevenson, P. C.; Hillier, J. *Discuss. Faraday Soc.* 1951, *11*, 55–75.

[20] Frens, G. *Nature Physical Science* 1973, *241*, 20–22.

[21] Snowden, M. E.; Güell, A. G.; Lai, S. C. S.; McKelvey, K.; Ebejer, N.; O'Connell, M. A.; Colburn, A. W.; Unwin, P. R. *Anal. Chem.* 2012, *84*(5), 2483–2491.

[22] Lai, S. C. S.; Patel, A. N.; McKelvey, K.; Unwin, P. R. *Angew. Chem.* 2012, *124*(22), 5501–5504.

[23] Güell, A. G.; Ebejer, N.; Snowden, M. E.; McKelvey, K.; Macpherson, J. V.; Unwin, P. R. *Proc. Natl. Acad. Sci. USA* 2012, *109*(29), 11487–11492.

[24] Ebejer, N.; Schnippering, M.; Colburn, A. W.; Edwards, M. A.; Unwin, P. R. *Anal. Chem.* 2010, *82*(22), 9141–9145.

[25] Angerstein-Kozlowska, H.; Conway, B.; Barnett, B.; Mozota, J. *J. Electroanal. Chem. Interfac. Electrochem.* 1979, *100*(1-2), 417 – 446.

[26] Lai, S. C.; Kleijn, S. E.; Öztürk, F. T.; van Rees Vellinga, V. C.; Koning, J.; Rodriguez, P.; Koper, M. T. *Catal. Today* 2010, *154*(1-2), 92 – 104.

[27] Bard, A. J.; Faulkner, L. R. *Electrochemical Methods: Fundamentals and Applications, 2nd Edition;* Wiley, New York, 2001.

[28] Kleijn, S. E. F.; Serrano-Bou, B.; Yanson, A. I.; Koper, M. T. M. *Langmuir* 2013, *29*(6), 2054–2064.

[29] Karp, S.; Meites, L. *J. Am. Chem. Soc.* 1962, *84*(6), 906–912.

[30] Zare, H. R.; Nasirizadeh, N. *Electrochim. Acta* 2007, *52*(12), 4153 – 4160.

[31] Raoof, J.; Ojani, R.; Mohammadpour, Z. *Int. J. Electrochem. Sci.* 2010, *5*, 177–188.

[32] Álvarez-Ruiz, B.; Gómez, R.; Orts, J. M.; Feliu, J. M. *J. Electrochem. Soc.* 2002, *149*(3), D35–D45.